Morphology and Water Vapor Permeability of Temperature-Sensitive Polyurethanes

X. M. Ding,[1] J. L. Hu,[2] X. M. Tao,[2] C. P. Hu,[3] G. Y. Wang[3]

[1]*Fashion Art and Design Institute, Dong Hua University, Shanghai 200051, The People's Republic of China*
[2]*Institute of Textiles and Clothing, The Hong Kong Polytechnic University, Hong Kong, The People's Republic of China*
[3]*School of Materials Science and Engineering, East China University of Science and Technology, Shanghai 200237, The People's Republic of China*

Received 19 November 2006; accepted 13 May 2007
DOI 10.1002/app.27465
Published online 17 December 2007 in Wiley InterScience (www.interscience.wiley.com).

ABSTRACT: A series of segmented polyurethanes (PUs) were prepared, in which five different polyols and hexamethylene diisocyanate were used as soft segments, and 4,4′-diphenylmethane diisocyanate, hydrophilic segment poly (ethylene glycol) 200 (PEG 200), and chain extender 1,4-butanediol were used as hard segment. Morphology of the PUs was investigated using differential scanning calorimetry, wide angle X-ray diffraction, polarizing microscopy, and transmission electron microscopy. Water vapor permeability of the membranes as a function of temperature was tested accordingly. Results show that the presence of PEG200 interferes the crystallization of hard segment in these PUs, and at the same time, increases phase compatibility between soft and hard segment in the PET-PU. It leads to a lower crystal melting temperature and degree of crystallinity of soft segment in the segmented PU than those of pure polyols, and no crystallization existing in hard segment. A morphological model is proposed, that is, aggregated soft-segment-rich domains can be observed clearly in the PUs with high crystallinity in soft segment, while identifiable hard domains are well-distributed in the soft segment domains in the PU with low crystallinity. Within the temperature range of crystal melting, water vapor permeability of the PU membranes increases significantly with increase of temperature. Such temperature-sensitive property is triggered by crystal melting of soft segment. © 2007 Wiley Periodicals, Inc. J Appl Polym Sci 107: 4061–4069, 2008

Key words: polyurethane; morphology; water vapor permeability; temperature-sensitive

INTRODUCTION

Temperature-sensitive polyurethane (TS-PU) is one novel type of smart polymers. The water vapor permeability (WVP) of its membrane can undergo a significant increase as temperature increases within a predetermined temperature range.[1–6] Such smart property enables this material to have a broad range of applications in textile industry, medicine, environmental fields, and so on.[7] For example, the clothing materials, laminated/coated with TS-PU membranes, can be used to produce an amphibious diving suit, which enabled wearers to be comfortable both in and out of the water.[8]

It is well known that many properties of a polymer, such as volume, enthalpy, modulus, heat conductivity, and so on, will take a sharp jump at phase transition temperatures, that is, at the glass–rubber transition temperature (T_g) and the crystalline melting temperature (T_m).[9–11] On the other hand, according to Fujita's theory,[12] the diffusion coefficient varies exponentially with the free volume of a polymer at constant temperature that can mathematically be expressed as eq. (1)

$$D = A_d \exp(-B_d/F_v) \quad (1)$$

Here, the parameter A_d depends mainly on the size and shape of the diffusive molecules and B_d on the minimum volume required for the displacement if diffusive molecules in the system. Extensive work has also shown the following expression [eq. (2)][13]:

$$P = A \exp(-B/F_v) \quad (2)$$

where A and B are constants for a particular gas. It is clear from equations that D and P increase with increasing free volume of the polymeric membrane.

As a result, the smart water vapor permeability of the TS-PU membranes mainly depends on the increase in the free volume in the transition temperature range, that is, depends on the microstructure and morphology of the materials. However, although some researchers started their research on the preparation of TS-PU, no morphological model was proposed to interpret such smart property till now.[14–17] Moreover, contradicting results were found on some research reports as concerned.[18] So, it is extremely desired to investigate the relationship between the morphology and water vapor permeability of TS-PU for preparing new tailor-made polymeric materials with specified properties.

Correspondence to: X. Ding (fddingxm@dhu.edu.cn).

Journal of Applied Polymer Science, Vol. 107, 4061–4069 (2008)

TABLE I
Notation and Composition of the Pus

	PEG200	PBA2000	PCL2000	PHA2500	PEA2200	PTMG2000	MDI	HDI	1,4-BDO
Content in feed (mol)									
PBA-15-PU	5.4	2.0					7.3	1.0	0.9
PCL-15-PU	5.4		2.0				7.3	1.0	0.9
PHA-15-PU	6.6			2.0			8.6	1.0	1.0
PEA-15-PU	5.8				2.0		7.7	1.0	0.9
PTMG-15-PU	5.4					2.0	7.3	1.0	0.9
PBA-20-PU	8.6	2.0					10.6	1.0	1.0
PBA-10-PU	3.0	2.0					4.8	1.0	0.8
Content in feed (wt %)									
PBA-15-PU	15.10	55.91					25.51	2.35	1.13
PCL-15-PU	15.10		55.91				25.51	2.35	1.13
PHA-15-PU	15.10			57.34			24.61	1.93	1.03
PEA-15-PU	15.00				56.96		24.83	2.18	1.02
PTMG-15-PU	15.10					55.91	25.51	2.35	1.13
PBA-20-PU	20.02	46.20					30.80	1.94	1.04
PBA-10-PU	10.08	65.95					20.02	2.77	1.19

For this purpose, in the present article, a series of PUs were prepared based on five different polyols and hexamethylene diisocyanate (HDI) as soft segments, and 4,4′-diphenylmethane diisocyanate (MDI), hydrophilic segment poly(ethylene glycol) 200 (PEG 200), and chain extender 1,4-butanediol (1,4-BDO) as blocked hard segment. Morphology of the PUs was characterized by differential scanning calorimetry (DSC), wide angle X-ray diffraction (WAXD), polarizing microscopy (POM), and transmission electron microscopy (TEM). Water vapor permeability of the membranes was measured at the temperature of 10, 15, 20, 30, and 40°C referring to ASTM E96-00. The relationship between the morphology and WVP of the TS-PUs was discussed accordingly.

EXPERIMENTAL

Materials

Five types of polyols, i.e., poly(butylenes adipate) 2000 (PBA 2000), polycaprolactone 2000 (PCL2000), poly(hexylene adipate) 2500 (PHA2500), poly(ethylene adipate) 2200 (PEA2200), and poly(tetramethylene glycol) 2000 (PTMG2000), were dried under vacuum at 110°C for 3 h. Poly(ethylene glycol) 200 (PEG 200) was dried at 80°C under vacuum for 4 h. The purified PEG 200 was dried further using 4 Å molecular sieve. 1,4-Butanediol (1,4-BDO) was distilled at 108°C under vacuum and dried further using 4 Å molecular sieve. *N*,*N*-Dimethylformamide (DMF) was distilled at 28°C under vacuum after dried using $MgSO_4$ for 24 h. Diphenyl methane 4,4′-diisocyanate (MDI) was filtered under vacuum and the fraction was received. Hexamethylene diisocyanate (HDI) was used as received.

Polyurethane synthesis

A series of segmented PU samples were synthesized using five different polyols. The formulas were listed in Table I. In a 500-mL four-necked flask, the polyol was reacted with HDI at 80°C for 2 h in the presence of dibutyl tin dilaurate (DBTDI) as a catalyst under nitrogen atmosphere. DMF was added to the reactor when necessary. Then PEG 200 and MDI were fed into the reactor sequentially and reacted for another 1 h at 80°C. Finally, 1,4-BDO was fed dropwise into the reactor at 60°C and reacted for 1 h. The PU solution was put into a PTFE model and kept for 16 h at 50°C, then for 24 h at 80°C, and finally for 8 h at 100°C under vacuum to make a film.

The structural formula of the PUs was shown as below:

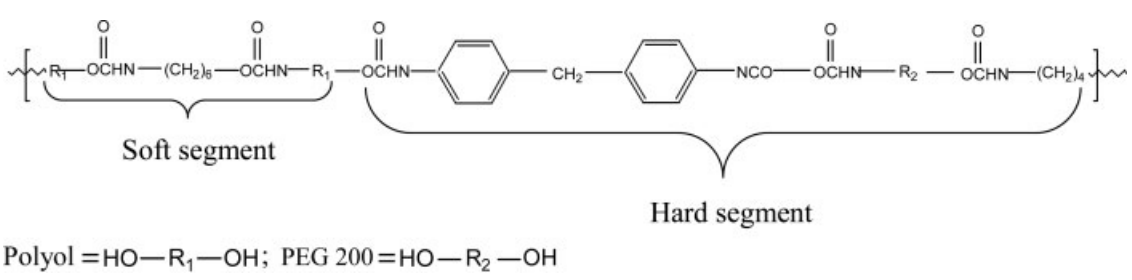

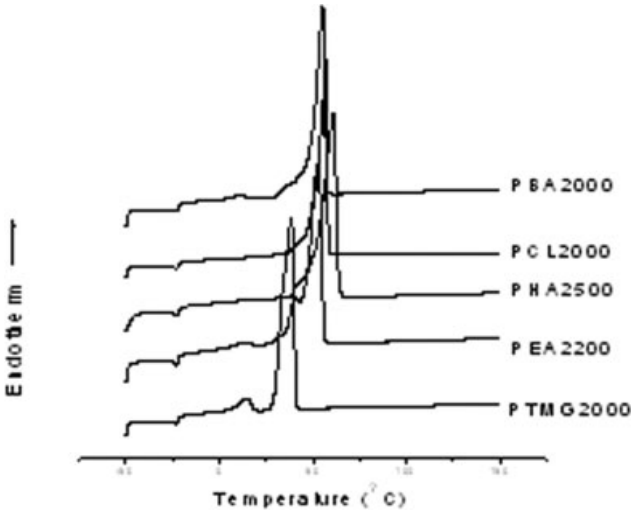

Figure 1 DSC results of five polyols.

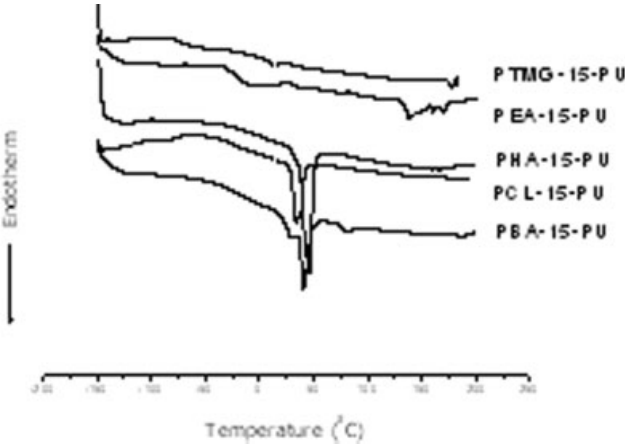

Figure 2 DSC scan plots for the PUs with different polyols as soft segment and 15% PEG content.

Polyurethane characterization

The thermal properties of the five types of polyols were measured using a Perkin–Elmer DSC7 and purged with nitrogen gas. The specimens were scanned from −50 to 150°C at a heating rate of 10°C/min. The weight of the specimens was 10.5–12.0 mg. The thermal properties of the resulting PUs were measured by a TA DSC 2910, modulated and purged with nitrogen gas. The specimens were scanned from −150 to 200°C at a heating rate of 10°C/min. The weight of the specimens was 6.5–9.0 mg.

Wide-angle X-ray diffraction (WAXD) traces were recorded in a D8 discover X-ray diffractometer (Bruker Axs GmbH Karisruhe, West Germany) at 40 kV and 40 mA, which was equipped with Goebel mirror and Cu Kα radiation with a wavelength of 1.542 Å. Diffraction patterns were obtained in the range of Bragg's angle $2\theta = 5$–40°.

A polarizing microscopy (POM) (Leitz Wetzlar) was used to observe the morphology of the PUs. Transmission electron micrographs (TEMs) were observed on a Hitachi H-800 Electron Microscope. The PU stick held by epoxy resin was cut by an ultra microtome. These specimens with about 50 nm in thickness were exposed on the vapor of the solution of RuO_4 at room temperature for 1 h. Then the stained specimens were observed with TEM.

Water vapor permeability of the membranes was measured referring to ASTM E96-00. That is, an open cup containing water was sealed with the specimen membrane, and the assembly was placed in a test chamber at the different temperature of 10, 15, 20, 30, and 40°C with a constant relative humidity of 50%. After sorption equilibrium was attained, the water lost within next 12 h was recorded.

RESULTS AND DISCUSSION

Morphology of the PUs

Figures 1–3 show the DSC curves of pure polyols and the resulting PUs, while Table II lists the thermal values of onset temperature (T_{im}), peak temperature (T_{pm}), end temperature (T_{em}), and heat of fusion (ΔH_f). It is evident that the five pure polyols are crystalline with sharp endothermic peaks. The double melting peaks in PEA2200 and PTMG2000 could be ascribed to different degree of ordering or size in the crystallites.[19] For the corresponding PUs, melting temperatures, particularly T_{pm}s, shift to lower temperature with a sharp decrease in ΔH_f. The shift factor of peak temperature (ΔT_{pm}) is obtained through the following equation.

$$\Delta T_{pm} = T_{pm-\text{polyol}} - T_{pm-\text{PU}} \tag{3}$$

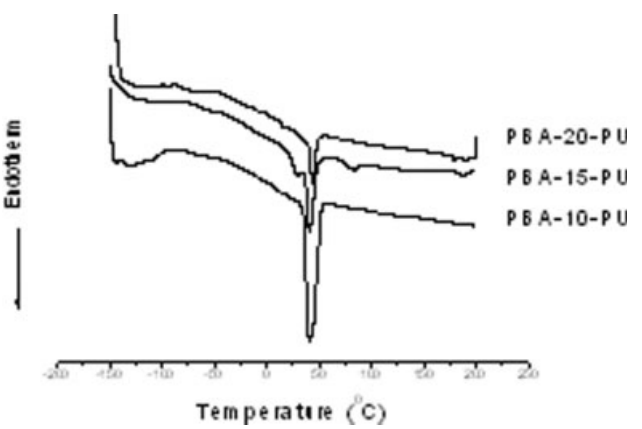

Figure 3 DSC scan plots for the PUs with PBA 2000 as soft segment and varied PEG contents.

TABLE II
Thermal Properties of the Polyurethanes

Samples	HSC (wt %)	T_{im} (°C)	T_{em} (°C)	T_{pm1} (°C)	T_{pm2} (°C)	ΔH_f (J/g)	ΔT_{pm} (°C)
PBA2000		29	59	55		81.30	
PCL2000		27	60	56		115.99	
PHA2500		37	67	61		106.97	
PEA2200		27	57	40	52	85.87	
PTMG2000		4	42	15	31	115.63	
PBA-10-PU	31	31	59	43		39.19	12
PBA-15-PU	42	11	66	32	41	26.81	14
PBA-20-PU	52	37	59	43		8.28	12
PCL-15-PU	42	18	50	35		26.46	21
PHA-15-PU	41	30	59	47		35.82	14
PEA-15-PU	41	N/A	N/A	N/A		N/A	N/A
PTMG-15-PU	42	7	27	16		1.48	15

where $T_{pm-\text{polyol}}$ is the peak temperature of polyol and $T_{pm-\text{PU}}$ is the peak temperature of the resulting PU. The result of ΔT_{pm} is also listed in Table II. So, it is clear that $T_{pm-\text{PU}}$ is 10°C lower than $T_{pm-\text{polyol}}$. With the increase in MDI+PEG content, ΔH_f of PBA-PUs decreases gradually, while their T_{pm} and ΔT_{pm} are very close.

WAXD results were shown in Figures 4–8 and Table III. Distances between parallel lattice planes of PUs are very similar to those of the corresponding pure polyols, while no crystalline peaks could be observed in the segmented PUs. It indicates that the crystallization was formed by polyols, while hard segment does not form crystallites in the segmented PU.[20] Degree of crystallinity (ω_c) of the PUs decreases sharply comparing to the corresponding pure polyols. Increase of the hard segment content (HSC) results in the decrease of ω_c of PBA-PUs. However, the presence of hard segment does not change the prominent peaks of crystalline polyols except that some secondary peaks disappeared. That is, effect of hard segment on crystallization of soft segment is selective. Only those crystallites growing in some special directions will be depressed sharply by hard segment until they disappear completely. For example, for PBA-based PUs (PBA-PUs), the introduction of hard segment depresses the crystallization of PBA2000 and makes two secondary peaks disappear. However, it does not change the distance at 0.370 and 0.410 nm of main crystalline planes.

As usual, an endothermic peak of hard segment (MDI/BDO) could be observed in PUs when HSC was more than 30 wt %.[21–25] Only when HSC is less than 30 wt %, the endothermic peak of hard segment will disappear.[21,26–28] In this study, although HSC of all PUs is more than 30 wt %, no endothermic peak of hard segment can be observed. It can be ascribed to the presence of the small molecular weight PEG200. The introduction of PEG200 interferes obviously the aggregation of MDI/1,4-BDO, which depresses the crystallization of hard segment accordingly.

POM micrographs shown in Figure 9 illustrate the morphology for these PUs. Well-formed spherulitic crystallites could be observed in the PUs except PTMG-15-PU. Among these crystalline PUs, PHA-

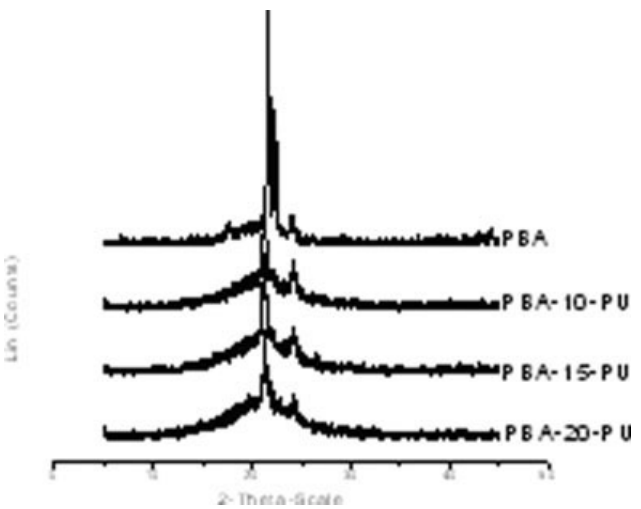

Figure 4 WAXD curves of PBA 2000 and PBA-PUs.

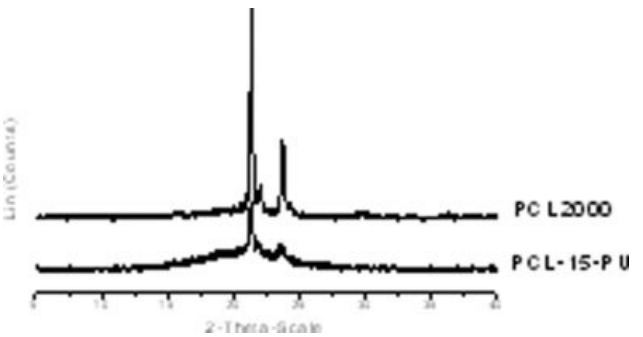

Figure 5 WAXD curves of PCL 2000 and PCL-15-PU.

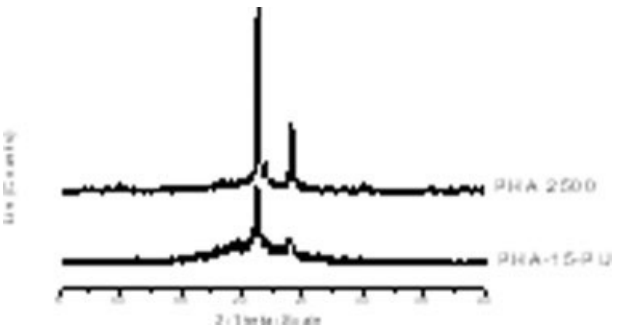

Figure 6 WAXD curves of PHA 2500 and PHA-15-PU.

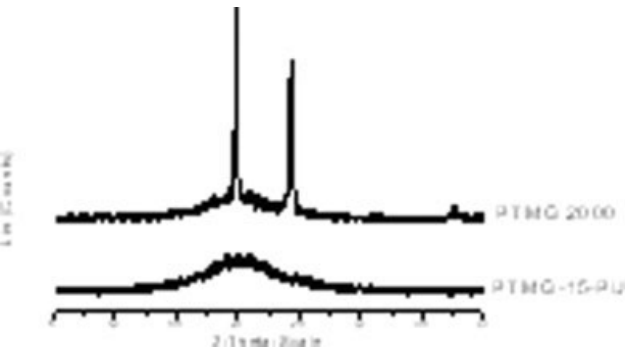

Figure 8 WAXD curves of PTMG 2000 and PTMG-15-PU.

15-PU and PBA-10-PU have larger spherulites about 20–40 μm in diameter, while PEA-15-PU and PBA-20-PU have smaller spherulites about 5–10 μm or less in diameter. PBA-15-PU has diameter of about 5–15 μm, and PCL-15-PU has diameter of about 10–30 μm. The increased HSC for PBA-PUs results in the decreased spherulites size, which can also be ascribed to the presence of small molecular PEG200.

Two-phase structure of these PUs is observed using TEM photos shown in Figure 10. After stained using RuO_4, the TEM micrographs reveal dark and white regions. The dark regions are ascribed to the hard segment due to the preferential attachment of RuO_4 to the urethane bonds in the hard segment.[29] The aggregation of soft/hard segments is distinct in PBA-15-PU and PHA-15-PU. The dark regions in the morphology of PBA-15-PU are smaller and more uniform than those in PHA-15-PU. It is probably related to the different ω_c, that is, the higher ω_c leads to the greater aggregation. For PTMG-15-PU, small domain morphology is distinct, which is ascribed to the aggregation of hard segment. In this PU, the white soft segment is assigned to continuous phase, while the dark hard segment is assigned to dispersed phase with an average diameter about 20–50 nm.

As reported, hydrogen bonding in polyester-based PU (PES-PU) is formed mainly between soft and hard segments, while hydrogen bonding in polyether-based PU (PET-PU) is formed mainly between hard segments. So the PES-PU presents greater phase miscibility than the PET-PU due to the stronger hydrogen bonding between the hard and soft segment.[30–32] However, in these PUs used in this article, it is obvious that the PES-PUs present greater phase separation than PET-PU. So it can be deduced that the additional hydrogen bonding in PET-PU is formed between polyether polyol (PTMG) and PEG200 due to the similar chemical structure. So the enhanced chemical linkage (connectivity) between hard and soft segment restricts the motion of crystalline polyols in the resulting PUs, which leads to the decrease in crystallinity of soft segment and promotes greater phase compatibility. By contrary, in PET-PU, some polar groups in MDI+BDO are used to compose hydrogen bonding with PEG200, which provides much chance for PES polyols to aggregate and results in phase separation, accordingly. DSC and WAXD results as above can support this deduction as well.

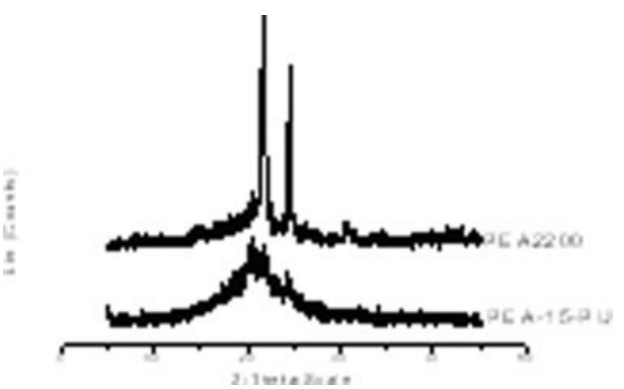

Figure 7 WAXD curves of PEA 2200 and PEA-15-PU.

TABLE III
Distance of Parallel Lattice Planes of Various Polyols and the Pus

	Distance between parallel lattice planes (nm)				
Sample no.	1	2	3	4	ω_c (%)
PBA 2000	0.410	0.398	0.370	0.306	68.5
PBA-10-PU	0.419		0.368		27.6
PBA-15-PU	0.418		0.368		24.8
PBA-20-PU	0.417		0.367		16.8
PCL 2000	0.416	0.404	0.375	0.366	65.4
PCL-15-PU	0.416	0.405	0.377		19.7
PHA 2500	0.416	0.405	0.368	0.297	75.1
PHA-15-PU	0.418		0.371		25.8
PEA 2200	0.409	0.362	0.210		48.0
PEA-15-PU	0.412	0.366		0.435	8.6
PTMG 2000	0.447	0.366	0.239		52.0
PTMG-15-PU	N/A	N/A	N/A	N/A	N/A

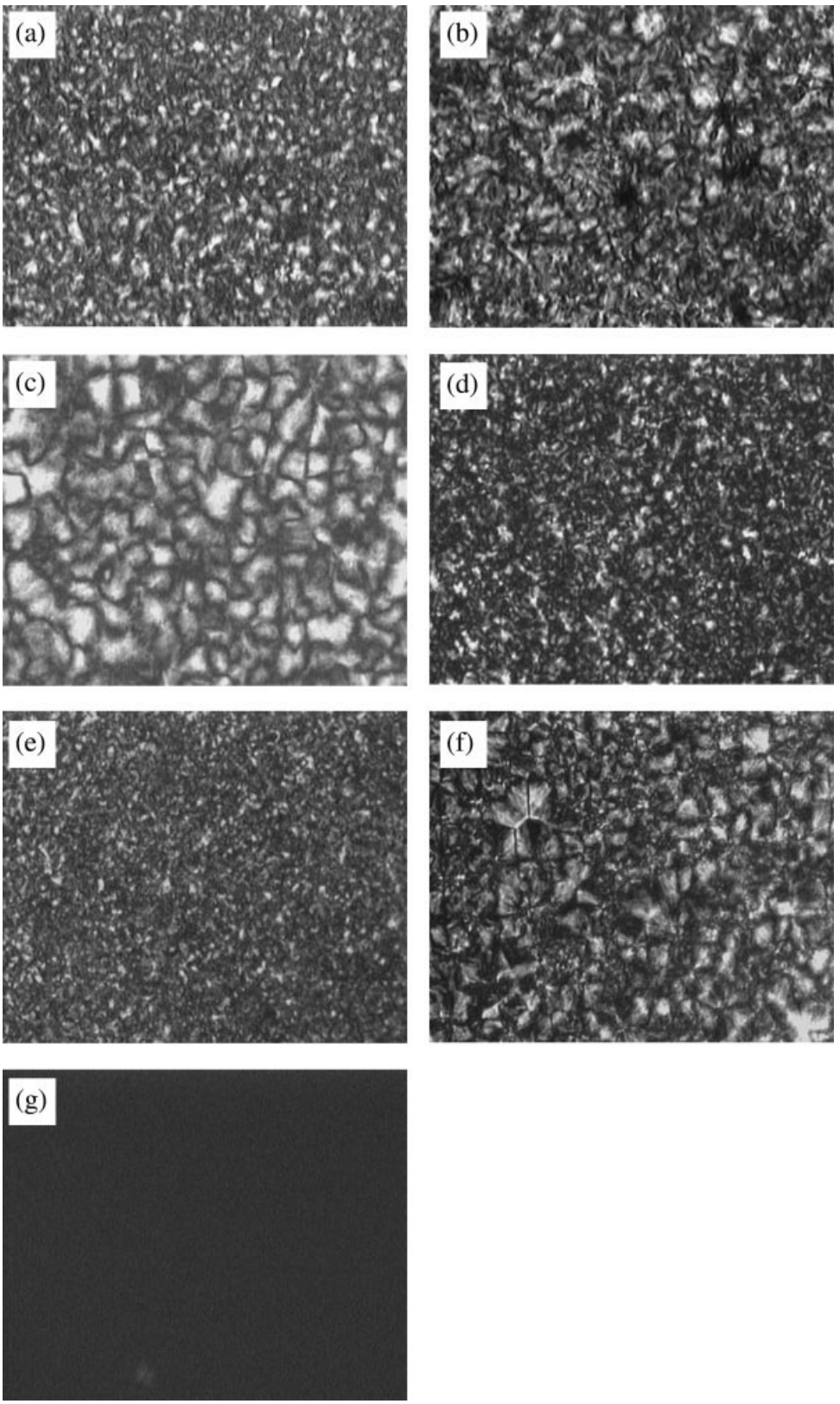

Figure 9 POM images: (a) PBA-15-PU; (b) PCL-15-PU; (c) PHA-15-PU; (d) PEA-15-PU; (e) PBA-20-PU; (f) PBA-10-PU; (g) PTMG-15-PU. Ruler: 30 μm.

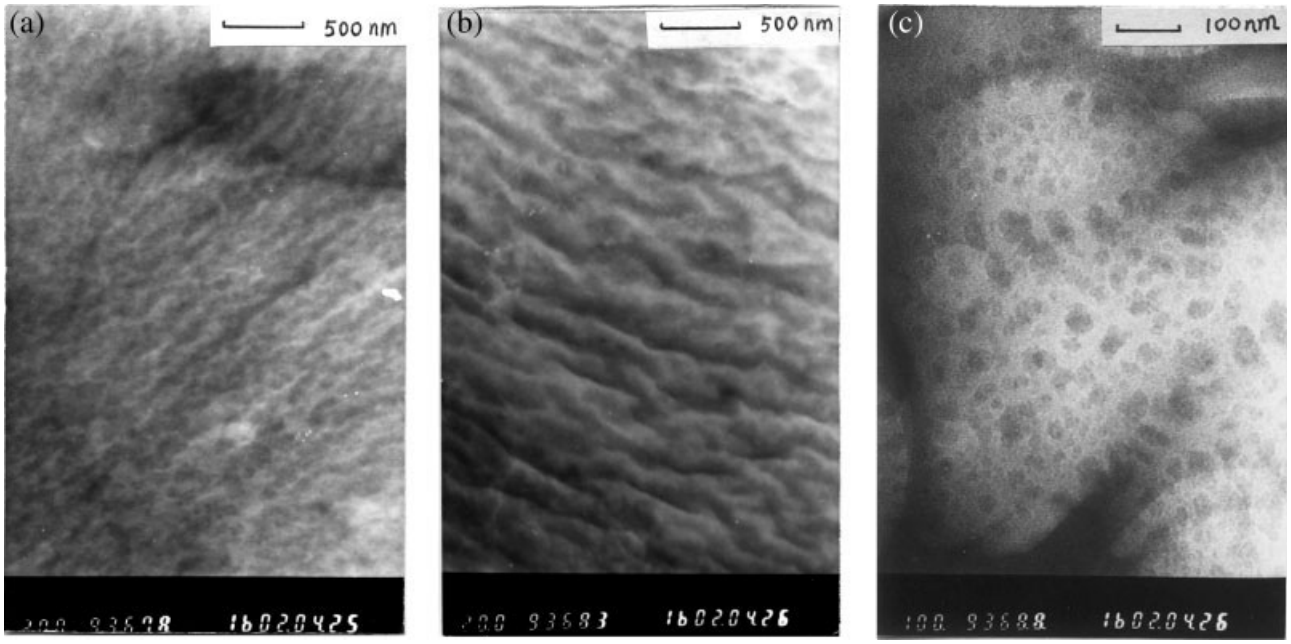

Figure 10 TEM microscopy: (a) PBA-15-PU; (b) PHA-15-PU; (c) PTMG-15-PU.

Water vapor permeability

Water vapor permeability (WVP) can be calculated using eq. (4) as follows.

$$\mathrm{WVP} = \frac{G}{tAS(R_1 - R_2)} \times l \tag{4}$$

where G = weight change; t = time during which G occurred; A = test area; S = saturation vapor pressure at test temperature; R_1 = relative humidity at the source expressed as a fraction; R_2 = relative humidity at the vapor sink expressed as a fraction; l = thickness of the membrane.

So the WVP of the PU membranes as a function of temperature is calculated and plotted on Figures 11 and 12. It is obvious that the WVP of these membranes except PTMG-15-PU increases significantly as temperature increases, while the WVP of PTMG-15-PU decreases in the same temperature range. Therefore, it is evident that PBA-PUs, PCL-15-PU, PHA-15-PU, and PEA-15-PU are temperature-sensitive in the measured temperature range from 10 to 40°C, while PTMG-PU is not.

It is well known that small penetrants pass a dense membrane through free volume between polymer molecules, mainly on soft segment region.[33] Therefore, the rate of permeation depends to a large extent on the size of penetrant and the free volume available. When the temperature is lower than T_{im}, the dense aggregation of soft segment in the crystalline PU leads to few water molecules through the membrane. With the increase in the temperature, the motion of soft-segment molecular chain triggered by crystal melting results in the significant increase in the free volume. Such significant increase in free

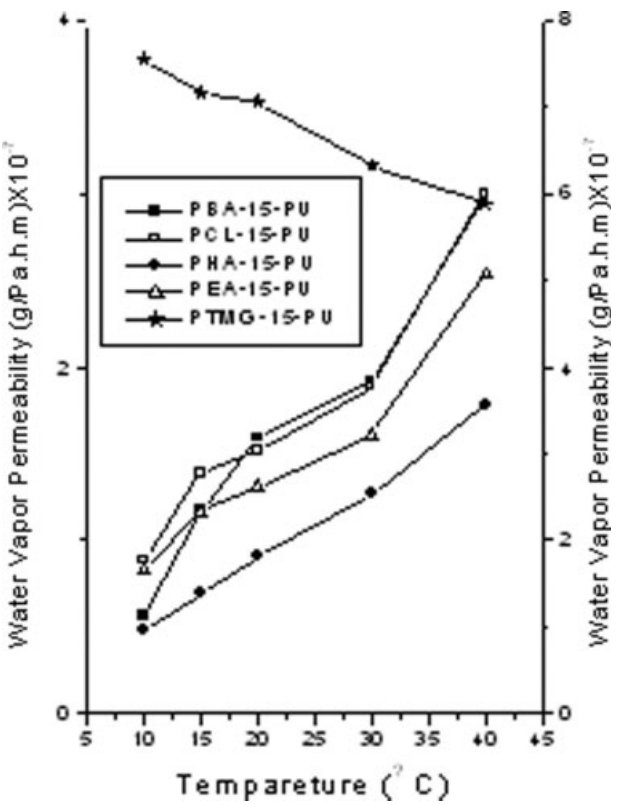

Figure 11 Water vapor permeability as a function of temperature of PUs with the similar HSC.

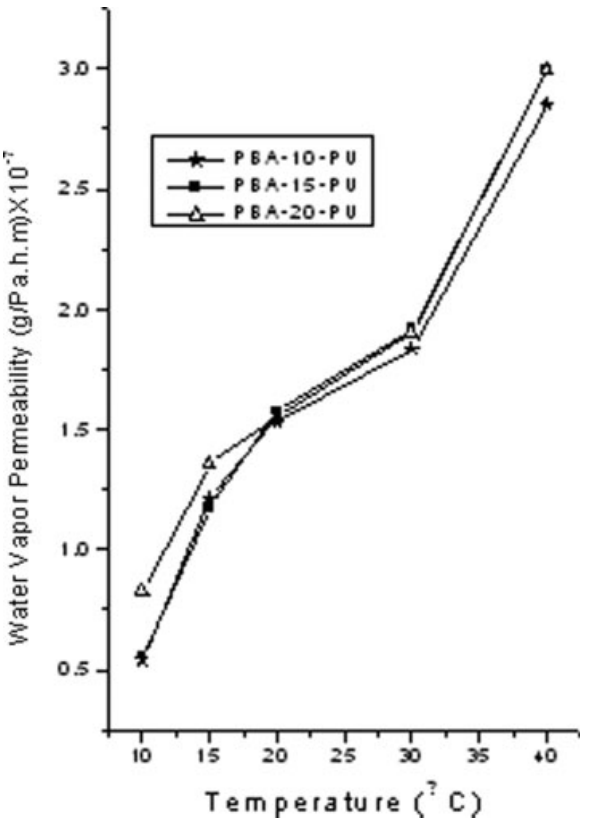

Figure 12 Water vapor permeability as a function of temperature of PBA-PUs.

volume can provide more paths for water vapor to pass through the membranes. That is, WVP increase significantly with the increase of temperature. For noncrystalline PU, the increased temperature does not trigger such significant increase in the free volume. So this type of PU cannot exhibit such smart behaviors. Based on the morphological study, these PES-PUs, such as PBA-PUs, PCL-15-PU, PHA-15-PU, and PEA-15-PU, are crystalline, while PTMG-15-PU is noncrystalline in the measured temperature range from 10 to 40°C. So in the predetermined temperature range, these PES-PUs exhibit smart behaviors in permeation of water vapor though the membrane, while PTMG-15-PU does not. In comparison with crystalline PES-PUs, the loose molecule structure in PTMG-15-PU provides more paths for water vapor transmission, which leads to large water vapor permeability.

CONCLUSIONS

Morphology of temperature-sensitive polyurethanes was investigated by DSC, WAXD, POM, and TEM. Water vapor permeability of the TS-PU membranes as a function of temperature was measured in the temperature range of crystal melting. The results show that the presence of PEG200 interferes the crystallization of hard segment in these PUs, and at the same time, increases phase compatibility between soft and hard segment in the PET-PU. It leads to a lower crystal melting temperature and lower degree of crystallinity of soft segment in the segmented PU than pure polyols, and no crystallization can be observed in hard segment. A morphological model is proposed, that is, aggregated soft-segment-rich domains can be observed clearly in the PUs with high crystallinity in soft segment, while identifiable hard domains are well-distributed in the soft segment domains in the PU with low crystallinity. Within the temperature range of crystal melting, water vapor permeability of the PU membranes increases significantly with increase in temperature. Such temperature-sensitive property is triggered by crystal melting of soft segment.

One of the authors, namely, Xuemei Ding would like to acknowledge a postgraduate scholarship from The Hong Kong Polytechnic University for this project.

References

1. Chen, G. H.; Hoffman, A. S. Nature 1995, 373, 49.
2. Grassi, M.; Yuk, S. H.; Cho, S. H. J Membr Sci 1999, 152, 241.
3. Stern, S. A. J Membr Sci 1994, 94, 1.
4. Ding, X. M.; Hu, J. L.; Tao, X. M.; Hayashi, S. Presented at the 6th Asia Textile Conference, Hong Kong, August 22–24, 2001.
5. Yoshida, R.; Uchida, K.; Kaneko, Y.; Sakai, K.; Kikuchi, A.; Sakurai, Y.; Okano, T. Nature 1995, 374, 240.
6. Lomax, G. R. Text Asia 2001, 32, 39.
7. Hayashi, S. Plast Eng 1995, 51, 29.
8. Graham-Rowe, D. In Going Commando; New Scientist Magazine, March, 2001; p 22.
9. Krevelen, D. W. v. Properties of Polymers: Their Correlation with Chemical Structure, Their Numerical Estimation and Prediction from Additive Group Contributions, 3rd ed.; Amsterdam: Elsevier, 1990.
10. He, M. J.; Chen, W. X.; Dong, X. X. Polymer Physics, 2nd ed.; Shanghai: Fudan University Publisher, 2000.
11. Gedde, U. W. Polymer Physics, 1st ed.; New York: Chapman and Hall, 1995.
12. Fujita, H. In Diffusion in Polymers; Crank, J.; Park, G. S., Eds.; Academic Press: New York, 1968.
13. Park, J. Y.; Paul, D. R. J Membr Sci 1997, 125, 23.
14. Hayashi, S. In Properties and Application of Polyurethane Based Shape Memory Polymer; Inoue, K.; Shen, S.; Taya, M., Eds.; Proceedings of the U.S.-Japan Workshop on Smart Materials and Structures; Mitsubishi Heavy Industries: Seattle, Washington, 1996.
15. Hayashi, S.; Ishikawa, N.; Giordano, C. J Coated Fabrics 1993, 23, 74.
16. Jeong, H. M.; Ahn, B. K.; Kim, B. K. Polym Int 2000, 49, 1714.
17. Jeong, H. M.; Ahn, B. K.; Cho, S. M.; Kim, B. K. J Polym Sci Part B: Polym Phys 2000, 38, 3009.
18. Gibson, P. Presented at the Fiber Society Annual Technical Conference, Natick, MA, USA, 2002.
19. Kloss, J.; Munaro, M.; De Souza, G. P.; Gulmine, J. V.; Wang, S. H.; Zawadzki, S.; Akcelrud, L. J Polym Sci Part A: Polym Chem 2002, 40, 4117.

20. Roe, R. J. Methods of X-ray and Neutron Scattering in Polymer Science; Oxford University Press: New York NY, 2000.
21. Zdrahala, R. J.; Gerkin, R. M.; Hager, S. L.; Critchfield, F. E. J Appl Polym Sci 1979, 24, 2041.
22. Foks, J.; Janik, H.; Russo, R. Eur Polym J 1990, 26, 309.
23. Lin, J. R.; Chen, L. W. J Appl Polym Sci 1998, 69, 1563.
24. Lin, J. R.; Chen, L. W. J Appl Polym Sci 1998, 69, 1575.
25. Ning, C. F.; He, C. Q.; Zhang, M.; Hu, C. P.; Wang, B.; Wang, S. J Acta Polym Sin 2001, 3, 299.
26. Zhu, Y. Q.; Huang, Y. Polym Mater Sci Eng 1994, 10, 80.
27. Li, F. K.; Hou, J. N.; Zhu, W.; Zhang, X.; Xu, M.; Luo, X. L.; Ma, D. Z.; Kim, B. K. J Appl Polym Sci 1996, 62, 631.
28. Bajsic, E. G.; Rek, V.; Sendijarevic, A.; Sendijarevic, V.; Frisch, K. C. J Elastomers Plast 2000, 32, 162.
29. Hua, F. J.; Hu, Ch. P. J Polym Sci Part A: Polym Chem 1999, 37, 3568.
30. Xiu, Y. Y.; Wang, D. N.; Hu, C. P.; Ying, S. K.; Li, J. X. J Appl Polym Sci 1993, 48, 867.
31. Sung, C. S. P.; Hu, C. B.; Wu, C. S. Macromolecules 1980, 13, 111.
32. Xiu, Y. Y.; Zhang, Z. P.; Wang, D. N.; Ying, S. K.; Li, J. X. Polymer 1992, 33, 1335.
33. Chen, C. X.; Han, B. B.; Li, J. D.; Shang, T. G.; Zou, J.; Jiang, W. J. J Membr Sci 2001, 187, 109.